Fluids and Barriers of the CNS

RESEARCH

Open Access

Ependymal cilia decline and AQP4 upregulation in young adult rats with syringomyelia

Longbing Ma[1†], Sumei Liu[1,2†], Qingyu Yao[1], Xinyu Wang[1], Jian Guan[1] and Fengzeng Jian[1,3,4,5,6*]

Abstract

Background Syringomyelia was a rare condition characterized by the formation of fluid-filled cysts (syrinx) within the spinal cord, resulting in sensory and motor dysfunction. Currently, there was no satisfactory treatment for syringomyelia. Ependymal cells were integral to water transport and may represent a promising therapeutic target.

Methods Induction of syringomyelia occurred in 8-week old female rats followed by histological analyses at 3-, 7-, 14-, 30-, 60-, 180-, and 365-days later. Scanning electron microscope (SEM) and transmission electron microscope (TEM) were performed to visualize cilia on rat central canal membrane cells at 30-day post-induction. Syringomyelia was induced via compression at T12-T13 using a sterile cotton ball. Each rat underwent MRI scanning one day before induction and one day prior to sacrifice. In vivo magnetic resonance imaging (MRI) was utilized to measure syrinx enlargement in eight-week-old syringomyelia rats. Histological Analysis and immunofluorescence staining were performed for changes of cilia, neurons, expression of AQP4 and infiltration of immune cells into spinal tissue.

Results In the current study, the cell junctions between ependymal cells of syringomyelia rats were absent, and the cilia on ependymal cells were reduced significantly on day 30 post syringomyelia. The number of ependymal cells kept increasing lasting for 1–2 months and begin to decrease. Edema and vacuolation in the spinal cord tissue are significant in syringomyelia rats. Furthermore, AQP4 expression was elevated in astrocytes of syringomyelia rats, and IBA1$^+$ immune cells infiltrated spinal tissue. Furthermore, neuronal necrosis began in the acute stage of syringomyelia, and reached its peak one month later. Pathological changes in axonal rupture at anterior commissure (connection of the left and right white matter) could be observed in syringomyelia spinal tissue.

Conclusions These findings underscored the significance of cilia on ependymal cells and the evolving microenvironment post-syringomyelia, providing valuable insights for clinical treatment strategies for this condition.

Keywords Cilia, Ependymal cell, Spinal cord injury, Syringomyelia, Rat, Neuronal necrosis

†Longbing Ma and Sumei Liu have contributed equally to this work.

*Correspondence:
Fengzeng Jian
jianfengzeng@xwh.ccmu.edu.cn
Full list of author information is available at the end of the article

Background

Syringomyelia is frequently defined as the development of an expansive, fluid-filled cyst within the spinal cord. Syringomyelia is associated with Chiari malformation, intramedullary tumor or spinal cord injury etc. [1–3]. Cavity formation within the spinal cord was first recognized by a pupil of Sylvius, Stephanus in 1545 and Charles-Prosper Ollivier d'Angers coined the term "syringomyelia" in 1827 [4]. Patients with syringomyelia usually present weakness of the arms or hands associated with a loss of pain and temperature sensation, and some may have neck discomfort related with also spine deformity, Charot joint and wound non-healing or long-term infection caused by denervation [5–8]. Despite the widespread attention given to this ancient disease, treatment options for syringomyelia remain limited [9, 10]. Clinicians often find themselves perplexed about how to treat syringomyelia, especially when it comes to neurological deficits such as pain, muscle atrophy in the limbs, alterations in pain and temperature sensation, and Charcot arthropathy [11]. Even with surgical intervention, many patients do not experience improvement in their syringomyelia [12], and surgical treatment often does not reverse any neurological deficits [13]. These symptoms, which significantly impact the survival and treatment of patients, appear to be irreversible. Moreover, surgery is invasive and is associated with a high risk of recurrence of the syrinx [14]. Therefore, it is crucial to elucidate the mechanisms underlying the development of syringomyelia and to explore experimental models in search of better therapeutic options.

Ependymal cells lining the central canal separate the cerebrospinal fluid (CSF) filling the cavity (such as ventricles, central canal of spinal cord) from the developing or mature spinal cord parenchyma. A prominent structural feature of ependymal cells is the cilia which beat in a coordinated manner to propel CSF flow. Cilia are divided into primary (9 + 0 microtubules) and motile cilia (9 + 2 microtubules) [15], and they show distinct structural and functional characteristics. Primary cilia are involved in sensing extracellular signals and are present on nearly all cells, in contrast, motile cilia are primarily present on the respiratory epithelium for example, and ependymal lining of the brain ventricles [16, 17]. Malfunctioning ependymal cilia could disrupt normal CSF flow, raising the risk of hydrocephalus. Dysfunction of normal cilia on the choroid plexus which produces CSF results in aberrant cAMP-regulated chloride transport, leading to enhanced fluid movement into the ventricle lumen and to excess CSF production [18]. Previous reports have shown ependymal cilia are required for directional migration of neuroblasts in brain [19]. In hydrocephalus, atrophy of ependymal cilia occurs prior to loss of ependymal cells [20], which reports participating in the pathogenesis of hydrocephalus in earlier studies [21, 22]. However, in the field of syringomyelia research, there is a limited amount of research investigating the roles of ependymal cilia due to the lack of appropriate animal models. Recently, we successfully established the rat syringomyelia models and found a reduction of cilia induced by loss of cell junctions and a proliferation of ependymal cells in syringomyelia [23–25]. Reports have shown that spinal cords with PTS displayed extracellular edema, cell death, loss of tissue integrity and alterations to endothelial tight junctions, suggested perturbations to blood-spinal cord barrier (BSCB) function [26]. Loss of cell junctions might lead to abnormal fluid infiltration, resulting in edema or cellular necrosis, as we hypothesized. Here we found the ciliary dysfunction of ependymal cells and edema of astrocytes around ependymal layer aggravate syrinx formation after syringomyelia, providing some important information for understanding the new insights of ependymal layer in central canal.

Methods

Experimental design

The experiment consisted of two groups (syringomyelia group and sham-operated group). After induction, the rats in the syringomyelia group were executed according to the time points (3 days, 7 days, 14 days, 1 month, 2 months, 6 months, and 12 months, n = 3/group at each time-point), and were subjected to immunohistochemistry and immunofluorescence staining. The longest observation time was 12 months after induction. Electron microscopy was used to visualize cilia on rat ventricular membrane cells at 30 days. 7 T MRI was used to dynamically visualize changes in syrinx at multiple time points.

Animal care and ethics statement

Eight-week old female Sprague Dawley (SD) rats weighing 250–300 g were purchased (Charles River, China) for this study. The rats were housed in standard sterile pathogen-free facilities (temperature: 24 ± 2 °C, humidity: 50–60%, 12-h light/dark cycle) with free access to food and water. All of the animal experiments were approved and performed in accordance with the standards of the Experimental Animal Center of Xuanwu Hospital Capital Medical University (no. XWH2019002).

Surgical procedure

The detailed surgical procedure was performed according to our previously published methods [25]. Briefly, the rats were anesthetized byenflurane inhaling anesthesia (2% enflurane in 70% nitrous oxide and 30% oxygen), and a 3-cm skin incision was performed on the back. Retracted the paravertebral muscle of T12-L1with micro-retractor

(LOGAN 3×3, RWD, Shenzhen, China) under a surgical microscope (OPMI pico, Carl Zeiss, Oberko Chen, Germany). Ligamentum flavum between the T12-T13 intervertebral space was cut by micro-scissors without injuring the dura. The integrity of dura must be protected and pay attention on CSF leakage. After the confirmation, a sterile aseptic cotton ball in an appropriate size was reshaped to a long strip and stuffed into the epidural space below the T13 lamina with a nerve stripper. After flushing with saline, muscles and skin were sutured and closed. Rats in normal group only received skin incision, muscle exposure and ligamentum flavum incision as same as the experimental group. After the surgery, antibiotics (cefuroxime sodium, Sinopharm group Zhijun pharmaceutical co. LTD, China) was injected intraperitoneally every 8 h for 1 week.

In vivo MRI and measurements of syrinx enlargement

Each rat was subjected to MRI scanning 1 day prior to induction and 1 day before at sacrifice. Detailed MRI parameter has been described in our previous report [25]. Briefly, all rats underwent serial MRI scanning according to the experiment roadmap. In vivo MRI was performed using a 7.0 Tesla MRI scanner (PharmaScan 7 T, Bruker Corp., Karlsruhe, Germany) with 400 mT/m gradients. Sagittal and axial T2 weighted images were acquired with the operation area as the center by using a fat-saturated RARE sequence. A rat volume coil with a diameter of 89 mm was used for transmission and to obtain data. Each MRI scan took about 12 min. In the axial T2-weighted images of all rats, the anteroposterior diameter and circular area of the largest syrinx was measured. The anteroposterior diameter and circular area of the spinal cord at the same level was also measured. The ratio of syrinx area to spinal cord area at the same level was calculated to evaluate the enlargement of the syrinx dynamically. All measurements were made using the Horos software platform (v3.3.5, https://horosproject.org).

Histological analysis

After the animals were killed by overdose of pentobarbital sodium (150 mg/kg IP) according to the experimental roadmap, the animals were perfused with 4% paraformaldehyde in 0.01 mol/L Phosphate buffered saline (PBS), and the whole spinal column was removed after adequate perfusion and fixed in 4% paraformaldehyde for 24 h. Then, the spinal cord was removed carefully. The integrity of spinal cord and dura mater needs to be guaranteed. After dehydration, the spinal cord was embedded in melted paraffin and then sectioned at a thickness of 3 μm in the axial plane. Sections were stained with hematoxylin and eosin (H&E). On the axial plane of the largest syrinx, the area of central canal and spinal cord were measured at the maximal diameter of the syrinx, and the ratio of central canal to spinal cord area was calculated to evaluate the size of syrinx histologically. Ependymal cell count was also performed on H&E-stained sections. All slices are scanned by a high-resolution scanner (Panoramic MIDI, 3DHISTECH, Hungary). Measurements were made in ImageJ with FIJI installed (NIH, https://imagej.nih.gov/ij/).

Immunohistochemistry and immunofluorescence staining

Since the syrinxes were located 1–2 segments cephalad of the site of compression (i.e., segments T11-12), the spinal cord tissue used for immunohistochemistry and immunofluorescence staining was collected from this region. Then, spinal cord samples were fixed with 4% paraformaldehyde and cryoprotected with 30% sucrose. Twenty-micrometer spinal cord slices were obtained using a cryomicrotome. Slices were fixed in 4% paraformaldehyde for 15 min, and then washed three times with PBS with 0.1% Triton X-100. Slices were blocked with 5% bovine serum albumin (BSA) in PBS for 1 h, and incubated with the primary antibodies (diluted with 3% BSA) overnight at 4 °C. The primary antibodies used were rabbit anti-Tuj1 (CST, 5568S, 1:200), rabbit anti-IBA1 (Abcam, ab178847, 1:8000), rabbit anti-NeuN (CST, 24307S, 1:1000), rabbit anti-AQP4 (CST, 59678S, 1:200), and mouse anti-GFAP (CST, 3670 T, 1:200). Sections were washed three times and incubated in the corresponding secondary antibodies for 50 min. For immunohistochemistry staining, slices were stained with DAB chromogenic reagent and dehydrated. Images for immunofluorescence staining were visualized by a Zeiss 880 laser-scanning confocal microscope. Fluorescence results were measured by selecting 3 rats at least in each group. For each section, 9 positions were randomly selected to take pictures at confocal system, at the same parameters. And for each target protein, typical signals are chosen for cell counting, which is conducted using ImageJ software.

Scanning electron microscope (SEM) and transmission electron microscope (TEM)

For scanning electron microscopy, spinal cord tissue was harvested after perfusion with 4% paraformaldehyde from 1–2 segments cephalad of the site of compression (i.e., segments T11-12), and then fixed with 2.5% glutaraldehyde overnight. The tissue surrounding the central canal of the spinal cord was selected and trimmed to the size of 1 mm^3. The tissue was washed with PBS, and then fixed with 1% OsO4 solution for 2 h. The tissues were treated with the following solutions in sequence: PBS, 50% ethanol for 15 min, 70% ethanol overnight, 90% ethanol + 90% acetone for 15 min, 90% propanone for 15 min,

anhydrous propanone for 4×15 min, propanone-soaking agent intermixture for 4 h and pure soaking agent overnight. Then tissues were embedded, sliced, and stained. Images were captured using a scanning electron microscope (S-3400N, Hitachi, Japan) was used to observe, and were collected for analysis.

For transmission electron microscopy, the specimens were fixed in 2.5% glutaraldehyde solution for 2 h, washed with 0.1 mol/L PBS 3 times, and then dehydrated with 50%, 70%, 80% and 90% tert-butyl alcohol for 15 min respectively, and then dehydrated with 100% tert-butyl alcohol 3 times for 10 min. Then the samples were soaked in pure tert-butyl alcohol at 0 °C. After tert-butyl alcohol is crystallized, the sample is dried using a vacuum filter bottle. The sample was sprayed with gold by using an ion sputtering machine (IONSPUTTERJFC-1100). Images were captured using a transmission electron microscope (HT7700, Hitachi, Japan) at 100 kV, and collected for analysis.

Statistical analysis

GraphPad Prism 6 (GraphPad Software, San Diego, USA) was used for statistical analysis. Two-way repeated measures (RM) ANOVA followed by a post hoc test using the Tukey test was used for comparing syrinx size between two groups. If the data do not follow a normal distribution or exhibit homogeneity of variances, non-parametric tests (Kruskal–Wallis H test) was used for comparing number of AQP4+and $IBA1^+$ cells between the syringomyelia group and the control group. If the data meet the criteria for normal distribution (using the Shapiro–Wilk test) and homogeneity of variances (using Mauchly's test), ANOVA was used to compare the cell counts between two groups. All data are presented as means ± standard deviation (SD). $P < 0.05$ was considered statistically significant.

Results

Ependymal cilia decline in syringomyelia

Cellular connections between ependymal cells surrounding the central canal contain multiple types, such as adherens junctions, gap junctions and tight junctions. Our previous results have shown that deconstruction of gap junctions between ependymal cells initiated cilia decline in syringomyelia rats [23]. In the current study, cilia of the ependymal cells in syrinx were decreased sharply along the inner surface of the central canal, in contrast, dense cilia could be observed in normal rats (Fig. 1A). In syringomyelia rats, scanning electron microscopy revealed that two rostrocaudal adjacent syrinxes were interconnected, to facilitate the CSF flow under compression (Fig. 1B). A dilation of central canal could be observed between the syrinx, however, cilia seemed denser than that in syrinx (Fig. 1B). Furthermore, the morphologies of the residual cilia under syringomyelia were changed into lying and curling (Fig. 1C, left) with 9 + 2 microtubules of motile cilia remaining (Fig. 1C, right). Ependymal cells were bare in syringomyelia rats (Fig. 1D). Transmission electron microscope showed that cell junctions between ependymal cells were loose and broken (Fig. 1E).

Cilia decline might play roles on the proliferation of ependymal cells around central canal

Next we detected the proliferation of ependymal cells since forced induction/suppression of cilia can affect cell cycle progression [27]. We have previously have shown that ependymal cells proliferate in the acute stages of syringomyelia [24], however, it is not yet clear whether this is related to cilia decline. In the current study, ependymal cells around the central canal proliferated significantly from 3 days to 2 months after surgery to induce syringomyelia (Fig. 2A, B). In addition, MRI results and H&E staining showed that the syrinx kept expanding from day 3 to 12 months in syringomyelia rats (Fig. S1). Ependymal cells accumulated, protruded into the central canal and were loosely distributed around the central canal (Fig. 2A), which was consistent with previous report, showing a proliferation of ependymal cells by injection of kaolin into spinal cord [28]. At 6 and 12 months, ependymal cells surrounding a syrinx decreased significantly and were arranged more loosely by a single layer around the central canal (Fig. 2A and 1D). In normal rat spinal cord, the ependymal cells around the central canal are uniformly arranged. However, in syringomyelia rats, the ependymal cells around the central canal are not uniformly arranged. Frequently, there is cell aggregation in some areas, while cells are reduced and sparse in others. These changes continue for up to 6 months. The total cell count lining the central canal is more reflective of changes in the total number of ependymal cells rather than a localized area of the central canal. The number of ependymal cells gradually increased to 104 ± 9 from day 3 onward to 2 months in each section, and then decreased to 51 ± 8 at 12 months ($p < 0.0001$) (Fig. 2B). The number of ependymal cells gradually increased to 104 ± 9 from day 3 onward to 2 months in each section, and then decreased to 51 ± 8 at 12 months ($P < 0.0001$) (Fig. 2B). Our results suggest that reduction of cilia might induce proliferation of ependymal cells.

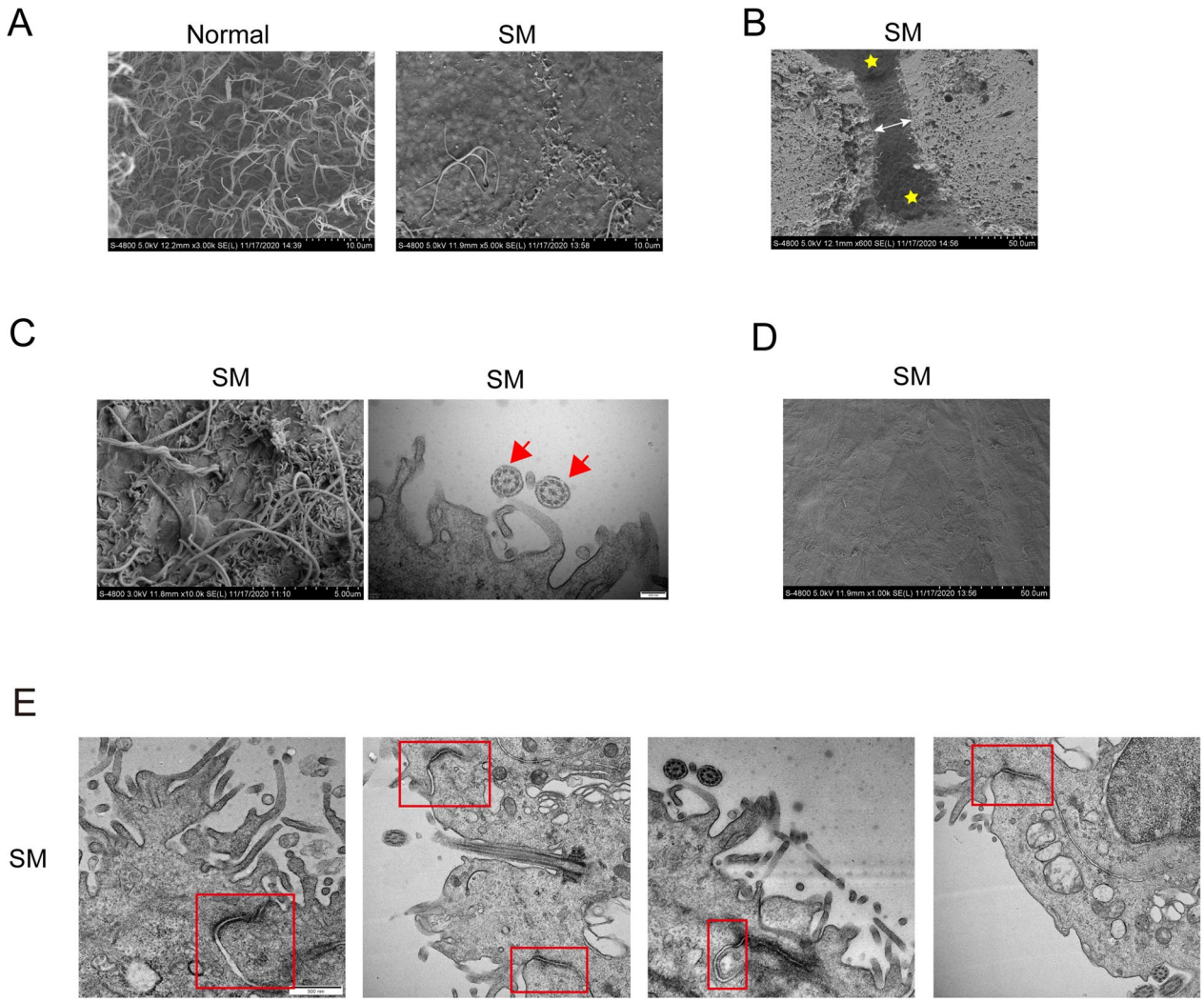

Fig. 1 Loss of cilia in ependymal cells of syringomyelia rats at day 30. **A**, Scanning electron microscope of the central canal in normal and syringomyelia groups. Dense cilia completely covered the inner surface of ependymal cells in normal rats and reduced sharply in syringomyelia rats. SM, syringomyelia. **B**, The connecting tunnel between two syringomyelia syrinxes were shown, with cilia decline in syrinxes. The yellow stars indicate syrinxes. Bi-directional arrows indicate dilation of central canal. **C**, Morphology of cilia in syringomyelia rats. The cilia are lying and winding seriously (left), and 9 + 2 microtubules could be seen (right). Red arrows indicate the 9 + 2 microtubules. **D**, The number of cilia on the inner surface of the central canal is greatly reduced in syringomyelia rats. **E**, Cell junctions between ependymal cells are loose and broken (red box), mitochondria and Golgi apparatus in ependymal cells are abnormal, and the nerve tissue adjacent to ependymal cells is severely edematous. The fourth small image in Figure 1E is another view of the same slice as the second small image.

Absence of cilia leads to elevated inflammatory response in syringomyelia

Ependymal cell might contribute to immunological processes [29]. In brain, the specialized ciliated ependymal cells lining the choroid plexus have tight junctions and form the blood-CSF barrier. Even though ependymal cells lining the central canal have adherens junctions and do not form a true barrier between CSF and spinal cord tissue, they are considered one of the main routes of cellular infiltration into the CNS during normal conditions, suggesting contribution to immunological processes. In our animal models, compression on the spinal cord induced ependymal cilia decline which subsequently resulted in the loss of ependymal cells, indicating destruction of immunological barrier under syringomyelia. We found $IBA1^+$ microglia cells in spinal cord of syringomyelia rats generally increased and showed amoeba-like activation (Fig. 3A). The number of $IBA1^+$ cells in the syringomyelia group was 2657 ± 389, while that in sham-operated rats was 354 ± 128 ($P < 0.0001$) (Fig. 3B). In addition, inflammatory cells, mainly macrophages, infiltrated into the cotton strips in the compressed spinal tissue (Fig. 3B). Our results show that syringomyelia induces an inflammatory response.

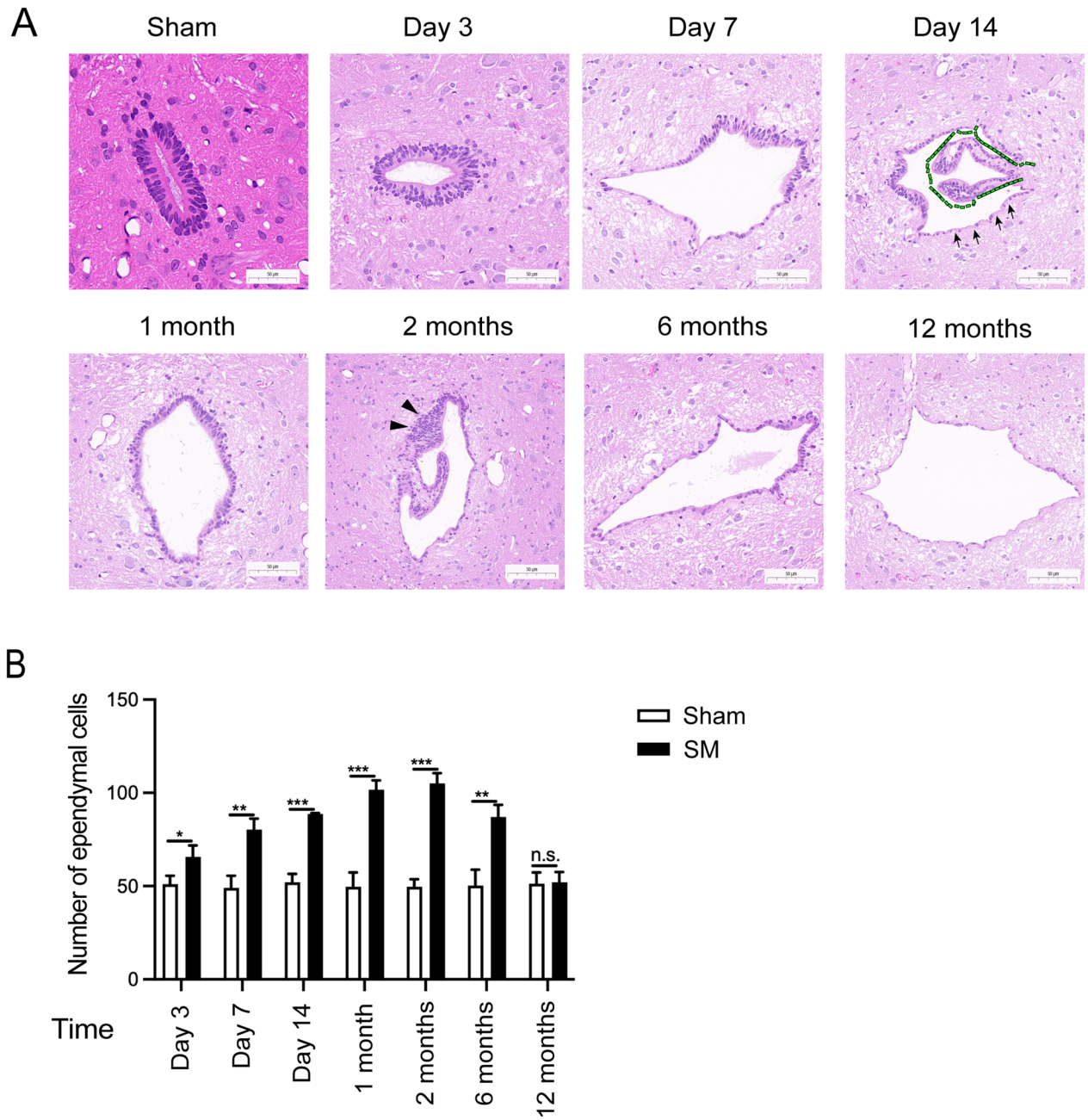

Fig. 2 Changes in ependymal cells in a rat model of syringomyelia at different time points. **A**, H&E stained images of spinal cord demonstrate that the syrinx gradually enlarged at each time point, and ependymal cells were unevenly distributed around the central canal. The number of local ependymal cells increased sharply and gathered. At 12 months, ependymal cells became very sparse. The dotted lines at Day 14, indicate ependymal cells protruding into the central canal and arrows indicate the loss of ependymal cells. Arrowheads indicate the proliferation of ependymal cells. **B**, The ependymal cell count showed the dynamic change of ependymal cell number around the central canal. *, $p < 0.05$; **, $p < 0.01$; ***, $p < 0.001$

Tissue edema and AQP4 upregulation around the syrinx in syringomyelia

Loss of functional cilia on ependymal cells exacerbated the abnormal CSF flow in the central canal, and may have led to excess CSF in the spinal parenchyma and subsequent tissue edema. H&E staining showed that there was a large area of edema around the syrinx, with a large number of necrotic cells in the ventral spinal tissue (Fig. 4A). By transmission electron microscope, we observed edema in the astrocytic foot processes adjacent

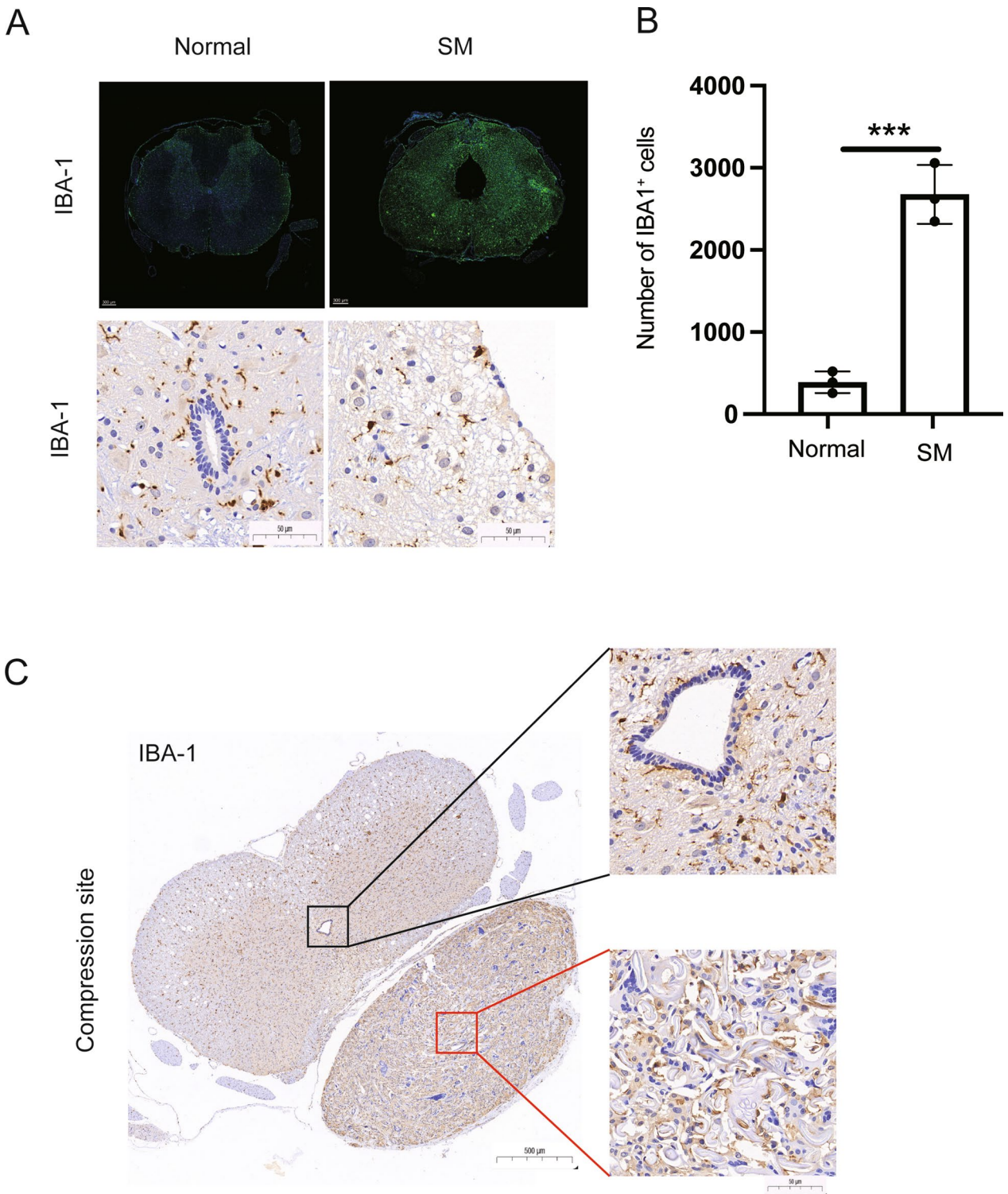

Fig. 3 Inflammatory response in a rat model of syringomyelia. **A**, Immunofluorescence and immunohistochemical staining of IBA1 indicated microglia proliferation and morphological changes in syringomyelia group. Scale bars, 300 μm. **B**, The count of IBA1 positive cell indicated that the number of microglia in syringomyelia group was significantly higher than that in control group. **C**, IBA1 staining of the spinal cord at the compressed part of cotton strip is used to distinguish the morphological differences of inflammatory cells in spinal cord tissue (black box) from cotton strip (red box) in epidural space. *$p < 0.05$; **$p < 0.01$; ***$p < 0.001$

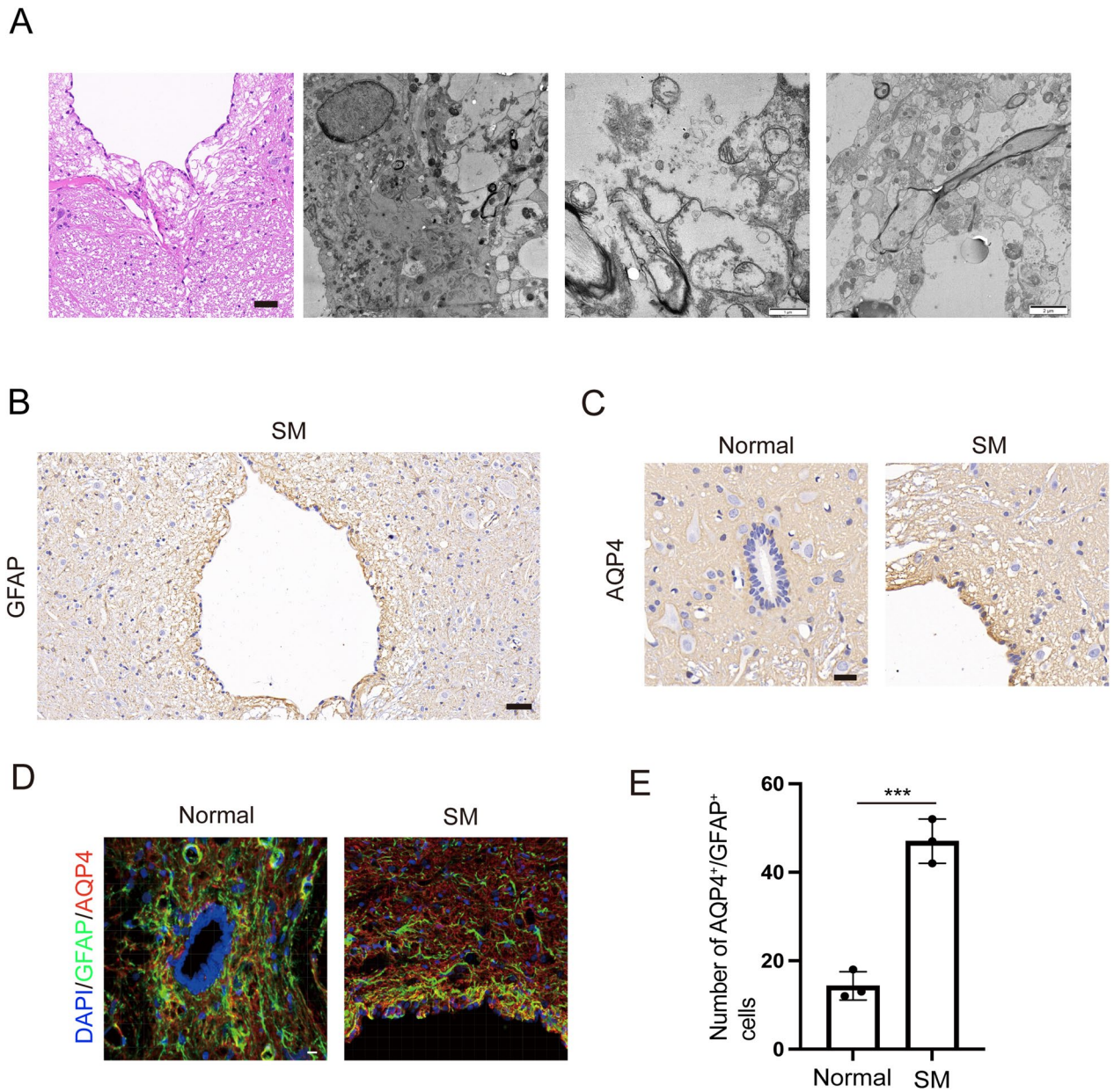

Fig. 4 AQP4 is overexpressed in syringomyelia. **A**, A large number of vacuoles and edema appeared around the central canal, and the tissue structure was obviously destroyed (left). Scale bar, 50 μm. Transmission electron microscopy of ependymal cells and spinal cord tissue around the central canal showed edema of astrocytic foot processes, cell necrosis, axonal injury and tissue disintegration (middle and right). **B**, $GFAP^+$ astrocytes around the central canal. Scale bar, 50 μm. **C**, Expression of AQP4 in cells around the syrinx was significantly higher than control group. Scale bar, 20 μm. **D**, AQP4 was co-stained with GFAP. Scale bar, 20 μm. **E**, The number of AQP4-positive cells was significantly higher in syringomyelia rats. *$p < 0.05$; **$p < 0.01$; ***$p < 0.001$

to the ependymal cells (Fig. 4A). At the same time, GFAP staining showed that there were a lot of vacuoles in the abnormal astrocytes in the tissues around the syrinx (Fig. 4B).

AQP4 is a water channel and has been shown to maintain CSF homeostasis [30]. AQP4 has been implicated in PTS. Expression of AQP4 at the syrinx border was strongly associated with syrinx size, while syrinx volume and length were not altered with AQP4 modulation, since the increases AQP4 levels was likely due to the increased number of reactive astrocytes, in which AQP was expressed [31]. AQP4 is expressed in astrocytes and has been proposed as a possible CSF biomarker for the diagnosis and prognosis of hydrocephalus [32]. Enhanced

AQP4 expression causes cytotoxic edema [33]. AQP4 deletion reduces spinal cord oedema and improves outcome after compression spinal cord injury in mice [34]. Reports have shown a significant higher expression of AQP4 around all syrinx cavities in post-traumatic syringomyelia [31, 35] and in spinal cord injury [36, 37]. AQP4 expression was significantly increased in the cells around the central canal, and concentrated in the 1–2 layers of cells lining the central canal (Fig. 4C) in rats with syringomyelia. $GFAP^+$ astrocytes around the central canal expressed AQP4 (Fig. 4D) and the number of $AQP4^+$/$GFAP^+$ positive cells was increased in syringomyelia (Fig. 4E). The results suggest that AQP4 may be involved in the alleviation of the enlargement of central canal in syringomyelia.

Neuronal necrosis and disorders of neural function in syringomyelia rats

A previous study demonstrated that AQP4 knockdown resulted in reduced spinal cord water content and recovery of sensory and locomotor function within 1 week following spinal cord injury [38]. In our study, we found that the central canal was obviously dilated, so that the gray matter of the spinal cord was compressed by the syrinx (Fig. 5A). The number of mitochondrial cristae decreased or even disappeared, and the mitochondria swelled obviously. In terms of morphology, we observed cilia lying, bending and winding together in the inner surface of central canal of the spinal cord. The number of neurons decreased as syringomyelia progressed (2 days to 12 months), most notably in the first 2 months, ranging from 423 ± 15 at 3 days to 403 ± 7 at 2 months (Fig. 5B). In the spinal cord gray matter surrounding the central canal, neurons displayed obvious characteristics of necrosis, such as disappearance of dendrites, pyknosis of nuclei, and vacuoles around cells (Fig. 5C). The number of necrotic neurons increased lasting for a long period and reached the peak at 1 month (24 ± 3), (Fig. 5D). Immunofluorescence staining of neurons showed the reduced neurons in syringomyelia spinal cord (Fig. 5E). Moreover, Tuj1 staining showed the conductive tract in the anterior commissural area of white matter were interrupted continuously (Fig. 5E). The transmission electron microscope of neurons showed that mitochondria of necrotic neurons with the disappeared cristae swelled obviously, and the Golgi apparatus appeared edema (Fig. 5G and Fig. S2). The axons were lamellar loosening, suggesting damage to nerve fibers (Fig. 5G). These findings suggest that syringomyelia induces spinal cord injury, leading to destruction of neural functions.

Overall, dysfunction of cilia on ependymal cells induced by syringomyelia lead to loss of ependymal integrity and neuron necrosis, which subsequently resulted in loss of neuronal function (Fig. 6). Our findings suggest that ependymal cilia play a crucial role in syringomyelia pathology and might be a potential target in clinical therapy.

Conclusion

Our results showed that reduction of cilia on ependymal cells, the infiltration of immune cell into spinal tissue and the increased necrotic neurons in syringomyelia rats, leading to secondary SCI. Upregulation of AQP4 in astrocytes may be involved in syringomyelia.

Discussion

In this study, we observed a significant reduction of cilia in ependymal cells at day 30 in a rat model of syringomyelia. However, the number of ependymal cells increased up until 1 month in animals with syringomyelia which was consistent with our previous reports [24] and decreased continuously from Day 7. Our colleagues have shown that cilia declined from day 7 to day 28 post syrinx induction [23], and the ependymal cells were proliferative and increased in the same period, presenting an opposite tendency. We hypothesized 2 possibilities to explain the finding: (1) the proliferation rate of ependymal cells with cilia cannot keep up with the rate of cilia shedding; (2)

(See figure on next page.)

Fig. 5 Syringomyelia leads to neuron necrosis and axonal injury around the central canal. **A**, The transverse sections of the spinal cord of syringomyelia rat were stained by immunohistochemistry and labeled with NeuN (high magnification insets of the areas delineated by the red boxes are shown in A1-A6). Neurons near the central canal of syringomyelia rats are sparsely distributed and abnormal in shape. **B**, The number of neurons in the transverse section of spinal cord showed that the number of neurons gradually decreased during the progression of syringomyelia. **C**, The gray matter neurons of the spinal cord around the central canal showed karyopyknosis, dendrite disappearance, vacuole around the cells and other necrosis phenomena (black arrows). The lower panels showed the high magnifications. **D**, The number of necrotic neurons around the central canal increased and this trend tends to be stable after one month. **E**, Immunofluorescence showed that neurons decreased (left) at 1 month of syringomyelia. Tuj1 immunofluorescence staining of spinal cord sections showed that the continuity of nerve fibers was interrupted in the anterior commissure of white matter (red box) adjacent to the syrinx (right), with low and high magnifications. Scale bar, 300 μm. DAPI, blue; NeuN and Tuj1, green. **F**, Diagram of nerve fibers. **G**, Transmission electron microscopy of spinal cord showed that mitochondria in neurons of normal (yellow arrow) and syringomyelia rats were swollen, disintegrated, cristae disappeared (red arrow), and Golgi apparatus was in edema state (red asterisk). *$p < 0.05$; **$p < 0.01$; ***$p < 0.001$

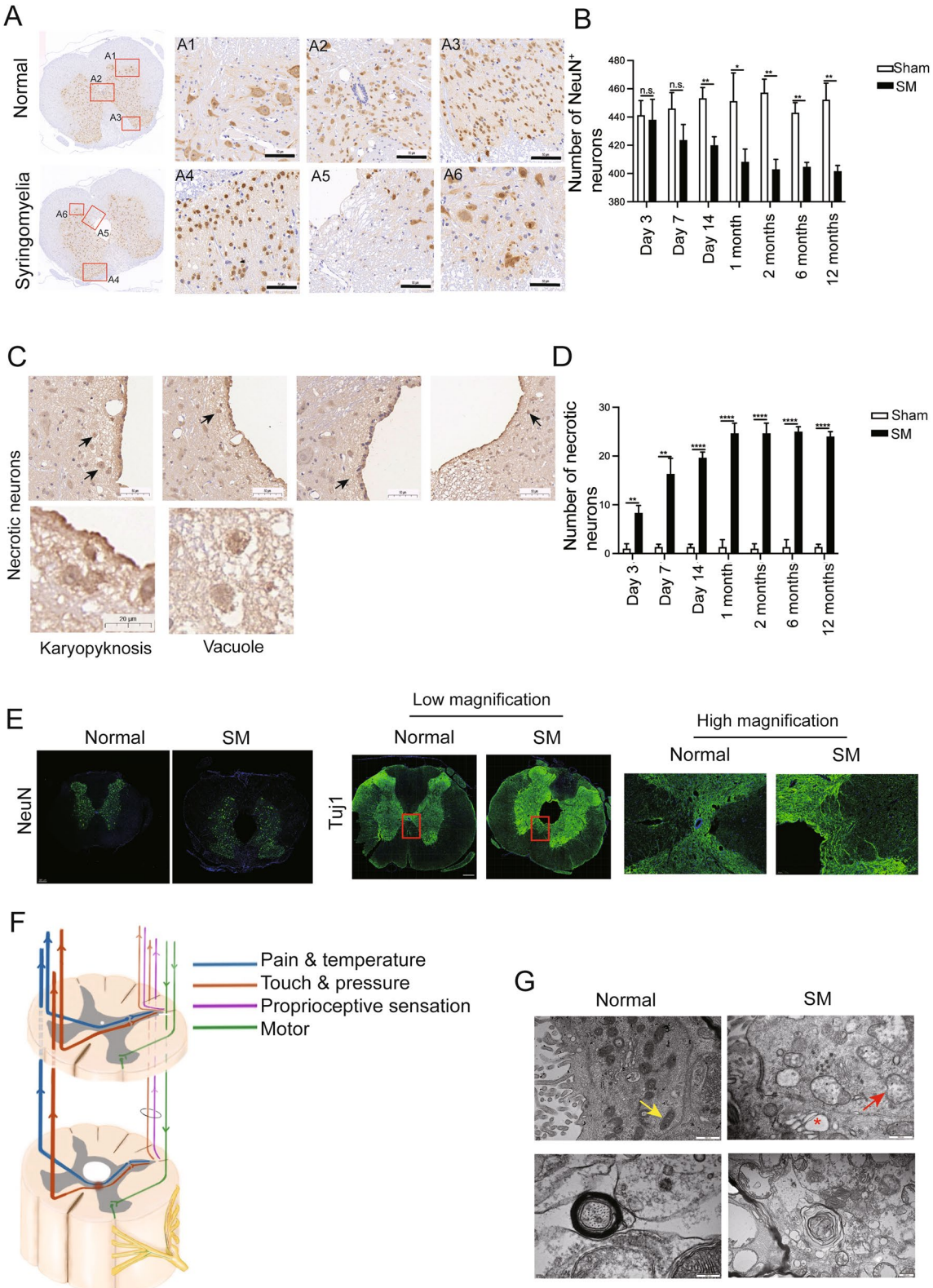

Fig. 5 (See legend on previous page.)

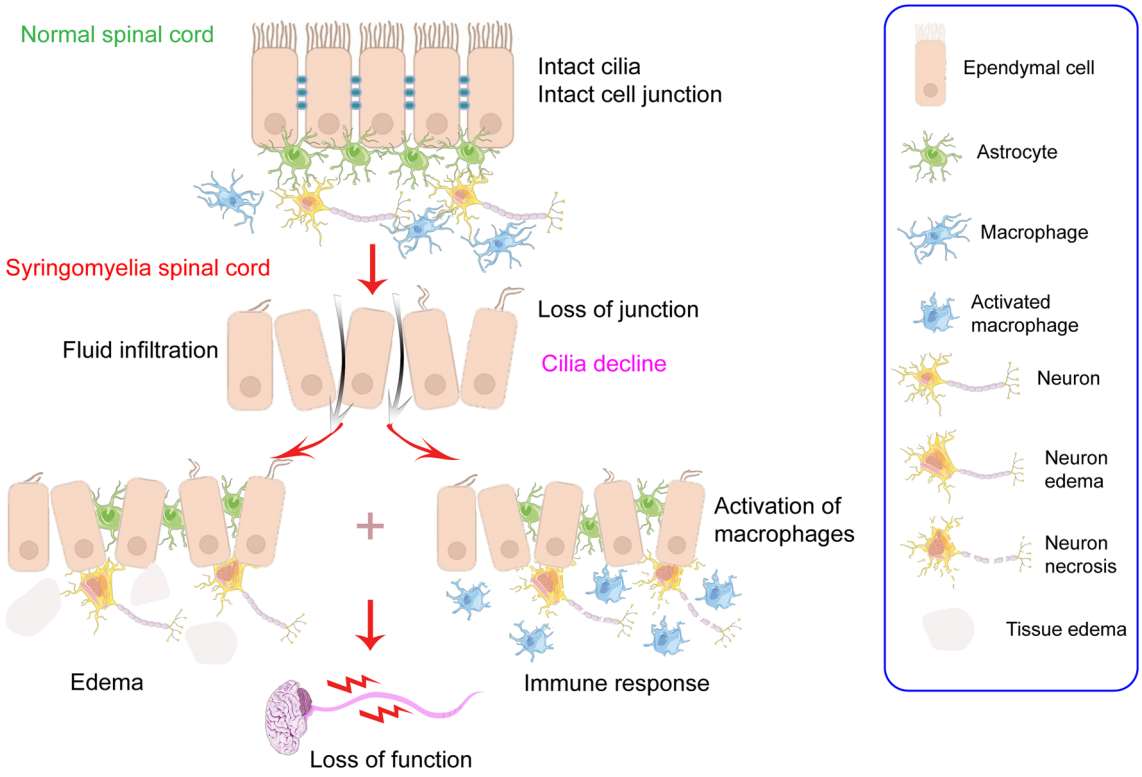

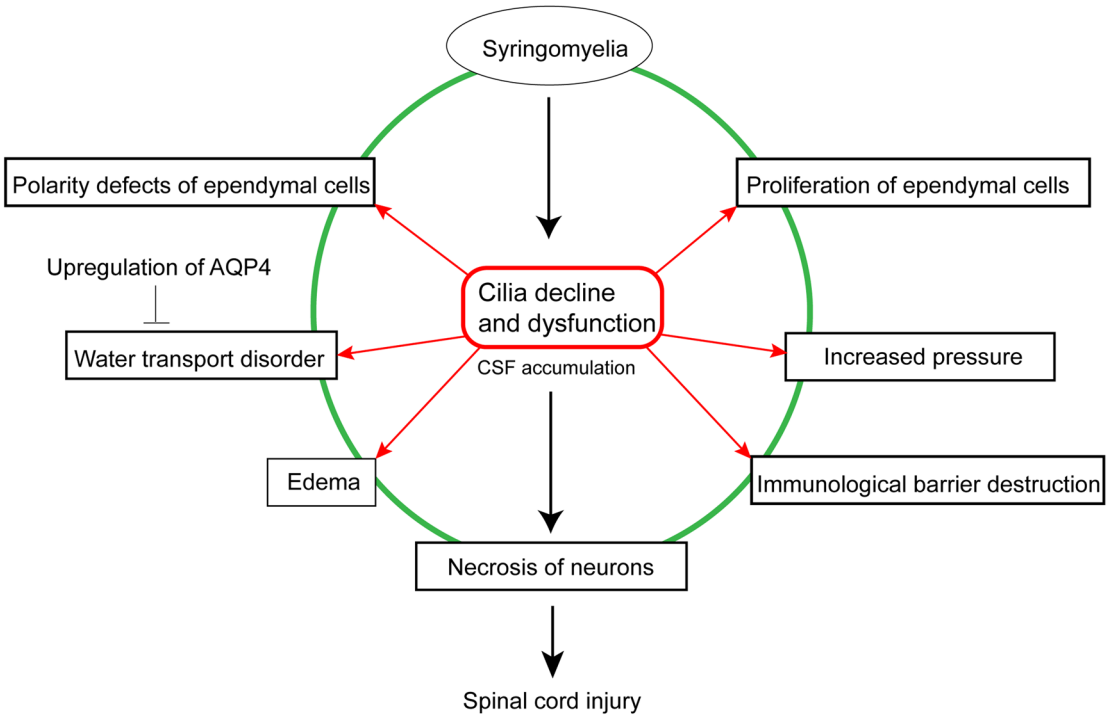

Fig. 6 Schematic diagram of secondary SCI induced by syringomyelia in our study. Cilia in ependymal cells played key roles during the process (upper). Cilia decline led to deconstruction of ependymal barrier and increased pressure in central canal. AQP4 upregulation may be a compensatory effect of spinal cord on water transport disorders like syringomyelia (lower)

the newly generated unhealthy ependymal cells lack cilia. These findings indicated loss of cilia might be involved in increase of ependymal cells and lead to dilation of central canal to form syrinx.

Increasing number of ependymal cells in syringomyelia might be associated cilia decline

Reports have shown that spinal cord stem cell potential is restricted to ependymal cells surrounding the central canal during adulthood, and silent/non-active ependymal cells are activated/proliferative by spinal cord injury [39–41]. In our study, we observed an increasing number of ependymal cells while a reduction of ependymal cilia. Reports have shown that cilia initiate disassembly as cells re-enter the cell cycle at G1-S transition [42–44], and are completely resorbed at early prophase [45], indicating ciliary dynamics control cell cycle entry or cell cycle progression. In addition, cilia grow from the centrosome that organizes the mitotic spindle during cell division, indicating that ependymal cell proliferation is associated with the assembly and disassembly of cilia. Previous studies have shown that forced retention of cilia imposes a brake on cell cycle progression [46]. Loss or dysfunction of cilia may allow activation of cAMP signaling which promotes cell cycle progression [45]. Furthermore, previous studies have indicated cilia in stem cells function as signal hub of pathways, including receptor tyrosine kinase (RTK), transforming growth factor-β (TGF-β), G-protein coupled receptor (GPCRs), Hedgehog (Hh), Wingless/int (Wnt), Notch, and mechanistic target of rapamycin (mTOR) [47–49]. For example, loss of cilia leads to activation of canonical Wnt and non-canonical Wnt/$Ca2^{+}$ pathways, implying cilia suppress Wnt signal [50] which is important for stem cells, including ependymal cells proliferation. Further investigation of interactions between cilia and proliferation of ependymal cells is needed in future.

Block of CSF flow by loss of cilia in ependymal cells may expedite syrinx formation

Ependymal cilia have a sensory function to regulate CSF homeostasis in central canal [17]. In the central canal, CSF-cNs (CSF-contacting neurons) possess an apical extension contacting the CSF to detect changes in CSF flow or content. PKD2L1 (polycystic kidney disease 2-like 1) was specifically expressed in CSF-cNs and played key roles on CSF dynamic and bending of the spinal cord during locomotion [51]. In syringomyelia, compression of the spinal cord results in impaired CSF flow. In addition, loss of cilia in CSF-cNs deprives of sensory function to block CSF flow, accelerating forcing dilation of central canal. Furthermore, partial accumulation of CSF in central canal may lead to high concentration of signals activating ependymal cells proliferation that would assist syrinx formation. We planned to employ single-cell transcriptome to explore more information regarding roles of CSF-cNs and PKD2L1 on monitoring CSF flow.

Aquaporin may be involved in the pathophysiological process of syringomyelia, which can be confirmed by previous studies [52] and the current study. We found a large amount of edema in the foot processes of astrocytes with increasing AQP4 expression around the central canal. moreover, disturbance to the homeostasis of ependyma is correlated with the formation of glial scar in both the brain and spinal cord [53] suggesting a spinal cord induced by syringomyelia. In our study, we found necrotic neurons increased and the total number of neurons decreased in spinal cord of rats with syringomyelia rats. Most patients with syringomyelia present with a characteristic sensory disturbance, that is, a decrease or loss of pain and temperature sensation. Spinal neuroanatomy suggests that this is due to the destruction of anterior white matter commissure where the nerve fibers from sensory neurons in the anterior horn of the spinal cord cross to the contralateral thalamic tract. Our results provide evidence of destruction of anterior white matter commissure in animal models that previous studies have not reported.

Clinically, even if patients with syringomyelia undergo surgery, their symptoms often remain. Combined with the findings of this study, this phenomenon may be related to the uncompensated injury of ependymal cells, which leads to irreversible spinal cord injury. Therefore, early intervention will be beneficial to most patients with syringomyelia, to prevent irreversible spinal cord injury.

Limitations

It should be noted that the animal model of syringomyelia used in the current study has several limitations. Firstly, our syringomyelia models do not accurately represented the clinical condition. The biggest limitation would be that the model used is representing the canalicular type of syringomyelia (a syrinx lined with ependymal cells) most often occurring in people with Chiari malformation. In this case the Chiari malformation is impairing CSF flow at the craniocervical junction, and a syrinx generally forms in the cervical spinal cord. Our model depicted in this study uses a compression at T12-T13 in rats to impair CSF flow and the syrinx formed at thoracic spinal cord. This does not accurately represent the clinical condition. In the future, we plan to improve animal models close to the clinical symptoms. Secondly, we did not use isometric time points to observe its morphological changes because the development of syringomyelia is slow post-op 2-month. We plan to add more time points in our further research to depict the spatiotemporal

changes of syringomyelia more precisely. Thirdly, we lack enough data to demonstrate the cause-and-effect relationship between cilia decline, activation of ependymal cells, edema, and AQP4 expression in syringomyelia. More trials should be carried out in the future. At last, the lack of gene experiments to directly verify the causes of syringomyelia and the difficulty of constructing gene knockout syringomyelia rats limit the exploration of the deep mechanisms.

Abbreviations

CSF	Cerebrospinal fluid
FOV	Field of view
IBA1	Ionized calcium binding adapter molecule 1
MRI	Magnetic resonance imaging
PBS	Phosphate-buffered saline
TR	Time of repetition
SCI	Spinal cord injury
SEM	Scanning electron microscope
TE	Time of echo
TEM	Transmission electron microscope

Supplementary Information

The online version contains supplementary material available at https://doi.org/10.1186/s12987-025-00631-2.

Additional file 1.

Acknowledgements
We acknowledge the help of Mr Jianfeng Lei, Mr Zhanjun Wang, Ms Wenqi Wu in the magnetic resonance imaging test in rats and image processing. We thank Prof. Wen Wang, and Mr Yufeng Wang of Xuanwu Hospital Animal Experiment Center for providing excellent technical support in the animal experiment. We are also grateful to Dr. Wenzheng Zou from Chinese Academy of Sciences for useful discussions and comments on the manuscript. We thank Dr. Cheng Lei for his great help in illustration.

Author contributions
Fengzeng Jian and Longbing Ma contributed to the study conception and design. Longbing Ma and Sumei Liu analyzed the data, drew the figures and write the manuscript. Longbing Ma, Qingyu Yao, Xinyu Wang and Jian Guan contributed to animal experiments, material preparation and data collection/analysis. Fengzeng Jian revised the draft and provided funding supports. All authors approved the manuscript.

Funding
This work was funded by National Natural Science Foundation of China (No. 82401591) and Beijing Natural Science Foundation (No. L212007).

Availability of data and materials
No datasets were generated or analysed during the current study.

Declarations

Ethics approval and consent to participate
All applicable international, national, and/or institutional guidelines for the care and use of animals were followed. All procedures performed in studies involving animals were in accordance with the ethical standards of the institution or practice at which the studies were conducted. (Experimental Animal Welfare Ethics Committee, Xuanwu Hospital, Capital Medical University, no. XWH2019002).

Consent for publication
Not applicable.

Competing interests
The authors declare no competing interests.

Author details
[1]Department of Neurosurgery, China International Neuroscience Institute, Xuanwu Hospital Capital Medical University, 45 Changchun Street, Beijing 100053, China. [2]Cell Therapy Center, Xuanwu Hospital Capital Medical University, 45 Changchun Street, Beijing 100053, China. [3]Spine Center, China International Neuroscience Institute (CHINA-INI), Beijing, China. [4]Lab of Spinal Cord Injury and Functional Reconstruction, Xuanwu Hospital, Capital Medical University, Beijing, China. [5]Research Center of Spine and Spinal Cord, Beijing Institute of Brain Disorders, Capital Medical University, Beijing, China. [6]National Center for Neurological Disorders, Beijing, China.

Received: 21 November 2023 Accepted: 10 February 2025
Published online: 24 February 2025

References

1. Giner J, Pérez López C, Hernández B, Gómez de la Riva Á, Isla A, Roda JM. Update on the pathophysiology and management of syringomyelia unrelated to Chiari malformation. Neurologia. 2019;34(5):318–25.
2. Blegvad C, Grotenhuis JA, Juhler M. Syringomyelia: a practical, clinical concept for classification. Acta Neurochir. 2014;156(11):2127–38.
3. Milhorat TH, Johnson RW, Milhorat RH, Capocelli AL Jr, Pevsner PH. Clinicopathological correlations in syringomyelia using axial magnetic resonance imaging. Neurosurgery. 1995;37(2):206–13.
4. Mortazavi MM, Rompala OJ, Verma K, Tubbs I, Tubbs RS, Cohen-Gadol AA. Charles prosper Ollivier d'Angers (1796–1845) and his contributions to defining syringomyelia. Childs Nerv Syst. 2011;27(12):2155–8.
5. Leclerc A, Matveeff L, Emery E. Syringomyelia and hydromyelia: current understanding and neurosurgical management. Revue Neurologique. 2021;177(5):498–507.
6. Bruzek AK, Starr J, Garton HJL, Muraszko KM, Maher CO, Strahle JM. Syringomyelia in children with closed spinal dysraphism: long-term outcomes after surgical intervention. J Neurosurg Pediatr. 2020;25(3):319–25.
7. Tosi U, Lara-Reyna J, Chae J, Sepanj R, Souweidane MM, Greenfield JP. Persistent syringomyelia after posterior fossa decompression for Chiari malformation. World Neurosurgery. 2020;136:454-461.e451.
8. Hayashi T, Ueta T, Kubo M, Maeda T, Shiba K. Subarachnoid–subarachnoid bypass: a new surgical technique for posttraumatic syringomyelia. J Neurosurg Spine. 2013;18(4):382–7.
9. Flint G. Syringomyelia: diagnosis and management. Pract Neurol. 2021;21(5):403–11.
10. Riordan CP, Scott RM. Fourth ventricle stent placement for treatment of recurrent syringomyelia in patients with type I Chiari malformations. J Neurosurg Pediatr. 2019;23(2):164–70.
11. Chakraborty U, Saha R, Roy U, Biswas A. Charcot arthropathy of elbow joint in syringomyelia. Neurol India. 2023;71(2):366.
12. Batzdorf U, Klekamp J, Johnson JP. A critical appraisal of syrinx cavity shunting procedures. J Neurosurgery. 1998;89(3):382–8.
13. Jian T, Liao J, Stoodley MA, Cunningham AM. Reaction of endogenous progenitor cells in a rat model of posttraumatic syringomyelia. J Neurosurgery-spine. 2011;14(5):573–82.
14. Lou Y, Yang J, Gu H, Xu G, Ji S, Xu C, Liu Y, Kim KG. A clinical study on the treatment of recurrent Chiari (Type I) malformation with syringomyelia based on the dynamics of cerebrospinal fluid. BioMed Res Int. 2022. https://doi.org/10.1155/2022/9770323.
15. Kumar V, Umair Z, Kumar S, Goutam RS, Park S, Kim J. The regulatory roles of motile cilia in CSF circulation and hydrocephalus. Fluids Barriers CNS. 2021. https://doi.org/10.1186/s12987-021-00265-0.
16. Satir P, Christensen ST. Overview of structure and function of mammalian cilia. Annu Rev Physiol. 2007;69(1):377–400.
17. Satir P, Christensen ST. Structure and function of mammalian cilia. Histochem Cell Biol. 2008;129(6):687–93.
18. Banizs B, Pike MM, Millican CL, Ferguson WB, Komlosi P, Sheetz J, Bell PD, Schwiebert EM, Yoder BK. Dysfunctional cilia lead to altered ependyma and choroid plexus function, and result in the formation of hydrocephalus. Development. 2005;132(23):5329–39.

19. Sawamoto K, Wichterle H, Gonzalez-Perez O, Cholfin JA, Yamada M, Spassky N, Murcia NS, Garcia-Verdugo JM, Marin O, Rubenstein JLR, et al. New neurons follow the flow of cerebrospinal fluid in the adult brain. Science. 2006;311(5761):629–32.
20. Bigio MRD. Neuropathological changes caused by hydrocephalus. Acta Neuropathol. 1993;85(6):573–85.
21. Saunders NR, Habgood MD, Dziegielewska KM. Barrier Mechanisms in the Brain, Ii. Immature Brain. Clin Exp Pharmacol Physiol. 1999;26(2):85–91.
22. Dziegielewska KM, Hinds LA, Møllgård K, Reynolds ML. Blood-brain, blood-cerebrospinal fluid and cerebrospinal fluid-brain barriers in a marsupial (Macropus eugenii) during development. J Physiol. 1988;403:367–88.
23. Wang X, Jiang C, Lu C, Ma L, Feng Y, Cui S, Li Q, Li K, Wang X, Jian F. Impairment of connexin 43 may initiate cilia decline in syringomyelia. Exp Neurol. 2023;365: 114430.
24. Liu S, Ma L, Qi B, Li Q, Chen Z, Jian F. Suppression of TGFβR-Smad3 pathway alleviates the syrinx induced by syringomyelia. Cell Biosci. 2023. https://doi.org/10.1186/s13578-023-01048-w.
25. Ma L, Yao Q, Zhang C, Li M, Cheng L, Jian F. Chronic extradural compression of spinal cord leads to syringomyelia in rat model. Fluids Barriers CNS. 2020. https://doi.org/10.1186/s12987-020-00213-4.
26. Berliner J, Hemley S, Najafi E, Bilston L, Stoodley M, Lam M. Abnormalities in spinal cord ultrastructure in a rat model of post-traumatic syringomyelia. Fluids Barriers CNS. 2020. https://doi.org/10.1186/s12987-020-0171-4.
27. Goto H, Inoko A, Inagaki M. Cell cycle progression by the repression of primary cilia formation in proliferating cells. Cell Mol Life Sci. 2013;70(20):3893–905.
28. Milhorat TH, Nobandegani F, Miller JI, Rao C. Noncommunicating syringomyelia following occlusion of central canal in rats experimental model and histological findings. J Neurosurg. 1993;78(2):274–9.
29. Jiménez AJ, Domínguez-Pinos M-D, Guerra MM, Fernández-Llebrez P, Pérez-Fígares J-M. Structure and function of the ependymal barrier and diseases associated with ependyma disruption. Tissue Barriers. 2014;2(1): e28426.
30. Trillo-Contreras JL, Ramírez-Lorca R, Villadiego J, Echevarría M. Cellular distribution of brain aquaporins and their contribution to cerebrospinal fluid homeostasis and hydrocephalus. Biomolecules. 2022;12(4):530.
31. Berliner JA, Lam MA, Najafi E, Hemley SJ, Bilston LE, Stoodley MA. Aquaporin-4 expression and modulation in a rat model of post-traumatic syringomyelia. Sci Rep. 2023. https://doi.org/10.1038/s41598-023-36538-x.
32. Castañeyra-Ruiz L, González-Marrero I, Hernández-Abad LG, Lee S, Castañeyra-Perdomo A, Muhonen M. AQP4, Astrogenesis, and hydrocephalus: a new neurological perspective. Int J Mol Sci. 2022;23(18):10438.
33. Lu H, Ai L, Zhang B. TNF-α induces AQP4 overexpression in astrocytes through the NF-κB pathway causing cellular edema and apoptosis. 2022. Biosci Rep. https://doi.org/10.1042/BSR20212224.
34. Saadoun S, Papadopoulos MC. Aquaporin-4 in brain and spinal cord oedema. Neuroscience. 2010;168(4):1036–46.
35. Hemley SJ, Bilston LE, Cheng S, Chan JN, Stoodley MA. Aquaporin-4 expression in post-traumatic syringomyelia. J Neurotrauma. 2013;30(16):1457–67.
36. Nesic O, Lee J, Ye Z, Unabia GC, Rafati D, Hulsebosch CE. Acute and chronic changes in aquaporin 4 expression after spinal cord injury. Neuroscience. 2006;143(3):779–92.
37. Oshio K, Binder DK, Yang B, Schecter S, Verkman AS, Manley GT. Expression of aquaporin water channels in mouse spinal cord. Neuroscience. 2004;127(3):685–93.
38. Kitchen P, Salman MM, Halsey AM, Clarke-Bland C, MacDonald JA, Ishida H, Vogel HJ, Almutiri S, Logan A, Kreida S, et al. Targeting aquaporin-4 subcellular localization to treat central nervous system Edema. Cell. 2020;181(4):784-799.e719.
39. Wu J, Tian WJ, Liu Y, Wang HJ, Zheng J, Wang X, Pan H, Li J, Luo J, Yang X, et al. Ependyma-expressed CCN1 restricts the size of the neural stem cell pool in the adult ventricular-subventricular zone. EMBO J. 2020. https://doi.org/10.15252/embj.2019101679.
40. Ren Y, Ao Y, O'Shea TM, Burda JE, Bernstein AM, Brumm AJ, Muthusamy N, Ghashghaei HT, Carmichael ST, Cheng L, et al. Ependymal cell contribution to scar formation after spinal cord injury is minimal, local and dependent on direct ependymal injury. Sci Rep. 2017. https://doi.org/10.1038/srep41122.
41. Li X, Floriddia EM, Toskas K, Fernandes KJL, Guérout N, Barnabé-Heider F. Regenerative potential of ependymal cells for spinal cord injuries over time. EBioMedicine. 2016;13:55–65.
42. Quarmby LM, Parker JDK. Cilia and the cell cycle? J Cell Biol. 2005;169(5):707–10.
43. Tucker RW, Scher CD. Stiles CD: centriole deciliation associated with the early response of 3T3 cells to growth factors but not to SV40. Cell. 1979;18(4):1065–72.
44. Kim S, Tsiokas L. Cilia and cell cycle re-entry. Cell Cycle. 2014;10(16):2683–90.
45. Pan J, Seeger-Nukpezah T, Golemis EA. The role of the cilium in normal and abnormal cell cycles: emphasis on renal cystic pathologies. Cell Mol Life Sci. 2012;70(11):1849–74.
46. Jackson PK. Do cilia put brakes on the cell cycle? Nat Cell Biol. 2011;13(4):340–2.
47. Mönnich M, Borgeskov L, Breslin L, Jakobsen L, Rogowski M, Doganli C, Schrøder JM, Mogensen JB, Blinkenkjær L, Harder LM, et al. CEP128 localizes to the subdistal appendages of the mother centriole and regulates TGF-β/BMP signaling at the primary cilium. Cell Rep. 2018;22(10):2584–92.
48. Clement Christian A, Ajbro Katrine D, Koefoed K, Vestergaard Maj L, Veland Iben R, de Jesus H, Maria Perestrello R, Pedersen Lotte B, Benmerah A, Andersen Claus Y, Larsen Lars A, et al. TGF-β signaling is associated with endocytosis at the pocket region of the primary cilium. Cell Rep. 2013;3(6):1806–14.
49. Álvarez-Satta M, Matheu A. Primary cilium and glioblastoma. Therap Adv Med Oncol. 2018;10:175883591880116.
50. Bae YK, Kim G-H, Kwon JH, Kim M, Choi SJ, Oh W, Um S, Jin HJ. Primary cilia mediate Wnt5a/β-catenin signaling to regulate adipogenic differentiation of human umbilical cord blood-derived mesenchymal stem cells following calcium induction. Tissue Eng Regen Med. 2020;17(2):193–202.
51. Sternberg JR, Prendergast AE, Brosse L, Cantaut-Belarif Y, Thouvenin O, Orts-Del'Immagine A, Castillo L, Djenoune L, Kurisu S, McDearmid JR, et al. Pkd2l1 is required for mechanoception in cerebrospinal fluid-contacting neurons and maintenance of spine curvature. Nature Commun. 2018. https://doi.org/10.1038/s41467-018-06225-x.
52. Zhang Y, Zhang YP, Shields LBE, Zheng Y, Xu X-M, Whittemore SR, Shields CB. Cervical central canal occlusion induces noncommunicating syringomyelia. Neurosurgery. 2012;71(1):126–37.
53. Rodríguez EM, Guerra MM. Neural stem cells and fetal-onset hydrocephalus. Pediatr Neurosurg. 2017;52(6):446–61.

Publisher's Note